Journal of Non-Newtonian Fluid Mechanics, 31 (1989) 301–323
Elsevier Science Publishers B.V., Amsterdam – Printed in The Netherlands

SIMILARITY SOLUTIONS THAT GIVE RISE TO HYPERBOLICITY AND CHANGE OF TYPE IN STEADY FLOW OF A VISCOELASTIC FLUID

CLAUDE VERDIER and DANIEL D. JOSEPH

Department of Aerospace Enginering & Mechanics, University of Minnesota, Minneapolis MN 55455 (U.S.A.)

(Received May 20, 1988; in revised form September 13, 1988)

Summary

Similarity solutions have proved to be a very useful tool for the study of flows of viscoelastic fluids since they allow us to check numerical computations against them. We compute here hyperbolic regions of the vorticity for an upper convected Maxwell model using the similarity solution of Phan-Thien for flow between rotating disks and using the similarity solution of Menon for an accelerated flow in cylindrical coordinates. We show that the extra tension becomes enormous at the edge of disks of ordinary rheometers under operating conditions.

1. Introduction

Phan-Thien [1,2] has found a similarity solution of an Oldroyd B fluid between parallel plates which rotate at different speeds around a common axis perpendicular to the plates. The solution is modeled according to a famous one by Von Karman in which the fluid variables are resolved into a quadratic polynomial in r with coefficients to be determined as functions of z. This problem is important because it may model the flow away from edges of the finite disks used in rheometers.

A different similarity solution for an upper convected Maxwell fluid has been given by Menon et al. [3]. Menon's problem is to determine the flow when the fluid is driven by an axisymmetric accelerated surface whose axial velocity w is proportional to the axial coordinate z. This kind of boundary condition is not a common one for devices which could be constructed but it is of interest in a subject where solutions so close to exact ones are so few.

0377-0257/89/$03.50

The work of Phan-Thien [1,2] and Menon [3] opens the door to the possibility of calculating transcritical steady flows of the upper convected Maxwell model, to which the Oldroyd B reduces when the Newtonian viscosity is put to zero, without linearizing and without relying completely on numerical methods. In each case we find an interesting transcritical flow.

We had hoped that the hyperbolic transitions could be identified with actual physical transitions as appears to be true in other problems. The neck-in instability at the free surface on a liquid sheared between rotating parallel disks is a candidate for such a transition because it occurs at a critical speed rather than at a critical shear rate. However the transcritical transition for the Maxwell model we used in our analysis occurs at a much higher one, orders of magnitude larger than what would be required to bring theory and experiment into agreement. We did more calculations than Phan-Thien and we found enormous stress components at what would be the edge of parallel plate rheometer in our analysis which neglects the ends.

The accelerated tube is not a problem that one can realize in an experiment so it is not possible to identify the physical transition that might be associated with a change of type.

On the computational side we motivate our work with the observation that similarity solutions are potentially useful tools for evaluating and improving numerical computations since they provide virtually exact solutions against which numerical calculations can be checked. Such exact solutions are test flows for numerical simulations in which the numerical problems are suspected to arise from a change of type.

2. Analysis of characteristics

We use the steady constitutive equations for an upper convected Maxwell model:

$$\lambda(\boldsymbol{u}\cdot\nabla\boldsymbol{\tau}-\boldsymbol{L}\boldsymbol{\tau}-\boldsymbol{\tau}\boldsymbol{L}^{\mathrm{T}})+\boldsymbol{\tau}=\eta(\boldsymbol{L}+\boldsymbol{L}^{\mathrm{T}}), \tag{1}_1$$

where $\boldsymbol{L}=\nabla\boldsymbol{u}$.

To this we append the equations of motion

$$\operatorname{div}\boldsymbol{u}=0, \tag{1}_2$$

$$\rho\boldsymbol{u}\cdot\nabla\boldsymbol{u}=-\nabla p+\operatorname{div}\boldsymbol{\tau}, \tag{1}_3$$

and write the whole system as a 10×10 matrix equation:

$$\boldsymbol{A}\boldsymbol{q}_r+\boldsymbol{B}\boldsymbol{q}_z=\boldsymbol{f} \tag{2}$$

for the system vector $\boldsymbol{q}=(u, v, w, \tau_{rr}, \tau_{r\theta}, \tau_{rz}, \tau_{\theta\theta}, \tau_{\theta z}, \tau_{zz})$ in cylindrical coordinates,

where $\boldsymbol{A}$ and $\boldsymbol{B}$ are given by

$$\boldsymbol{A} = \begin{bmatrix} -2a & 0 & 0 & 0 & u & 0 & 0 & 0 & 0 & 0 \\ -c & -a & 0 & 0 & 0 & u & 0 & 0 & 0 & 0 \\ -b & 0 & -a & 0 & 0 & 0 & u & 0 & 0 & 0 \\ 0 & -2c & 0 & 0 & 0 & 0 & 0 & u & 0 & 0 \\ 0 & -b & -c & 0 & 0 & 0 & 0 & 0 & u & 0 \\ 0 & 0 & -2b & 0 & 0 & 0 & 0 & 0 & 0 & u \\ \rho u & 0 & 0 & 1 & -1 & 0 & 0 & 0 & 0 & 0 \\ 0 & \rho u & 0 & 0 & 0 & -1 & 0 & 0 & 0 & 0 \\ 0 & 0 & \rho u & 0 & 0 & 0 & -1 & 0 & 0 & 0 \\ 1 & 0 & 0 & 0 & 0 & 0 & 0 & 0 & 0 & 0 \end{bmatrix},$$

$$\boldsymbol{B} = \begin{bmatrix} -2b & 0 & 0 & 0 & w & 0 & 0 & 0 & 0 & 0 \\ -d & -b & 0 & 0 & 0 & w & 0 & 0 & 0 & 0 \\ -e & 0 & -b & 0 & 0 & 0 & w & 0 & 0 & 0 \\ 0 & -2d & 0 & 0 & 0 & 0 & 0 & w & 0 & 0 \\ 0 & -e & -d & 0 & 0 & 0 & 0 & 0 & w & 0 \\ 0 & 0 & -2e & 0 & 0 & 0 & 0 & 0 & 0 & w \\ \rho w & 0 & 0 & 0 & 0 & 0 & -1 & 0 & 0 & 0 \\ 0 & \rho w & 0 & 0 & 0 & 0 & 0 & 0 & -1 & 0 \\ 0 & 0 & \rho w & 1 & 0 & 0 & 0 & 0 & 0 & 0 \\ 0 & 0 & 1 & 0 & 0 & 0 & 0 & 0 & 0 & 0 \end{bmatrix},$$

where a, b, c, d, e, are given by
$a = \tau_{rr} + G$, $b = \tau_{rz}$, $c = \tau_{r\theta}$, $d = \tau_{\theta z}$, $e = \tau_{zz} + G$ and $G = \eta/\lambda$ is the rigidity.

The characteristic surfaces are generated by the real values of $r' \overset{\text{def}}{=} \mathrm{d}r/\mathrm{d}z$ which satisfy

$$\det[\boldsymbol{A} - r'\boldsymbol{B}] = 0. \tag{3}$$

This leads to the following expression:

$$(u - r'w)^4(r'^2 + 1)(Ar'^2 - 2Br + C)^2 = 0, \tag{4}$$

where

$$\begin{aligned} A &= \rho w^2 - \tau_{zz} - G, \\ B &= \rho uw - \tau_{rz}, \\ C &= \rho u^2 - \tau_{rr} - G. \end{aligned} \tag{5}$$

We solved (3) using the symbolic manipulator program REDUCE2 on the Cyber. Streamlines are quartically characteristic.

Change of type is associated with the real roots of the last parenthesed part of expression (4). These roots are associated with the vorticity $\zeta = \zeta_\theta$.

$$A\frac{\partial^2\zeta}{\partial z^2} + 2B\frac{\partial^2\zeta}{\partial r\,\partial z} + C\frac{\partial^2\zeta}{\partial r^2} = \text{l.o.t.}, \tag{6}$$

where l.o.t. are lower order terms. The two other components ζ_r and ζ_z of the vorticity $\zeta = \text{curl } \boldsymbol{u}$ satisfy an equation of the same kind as (6) with the same left-hand side but different right-hand sides.

It follows that the projection of the characteristic surfaces of revolution onto the (r, z) plane are determined by integration of the equations

$$\frac{\mathrm{d}r}{\mathrm{d}z} = \frac{B \pm \sqrt{B^2 - AC}}{A} \tag{7}$$

in hyperbolic regions where $B^2 - AC > 0$.

3. Flow between parallel plates which rotate at different speeds around a common axis

We are now going to use the solutions given by Phan-Thien [1983] to determine the characteristics given by (7). The angular velocities of the lower and upper plates are Ω_1 and Ω_2. The distance between the plates is d, $Re = \Delta\Omega d^2/\nu$ is the Reynolds number where

$$\Delta\Omega \overset{\text{def}}{=} \Omega_2 - \Omega_1 \tag{8}$$

and $W = \lambda\,\Delta\Omega$ is the Weissenberg number. There are ten unknowns, six stresses, three velocities and the pressure. After introducing the similarity variable

$$\xi = z/d, \tag{9}$$

Phan-Thien derives ten equations for the velocity functions $h(\xi)$, $g(\xi)$ and the eight stress-like quantities with hats which are listed below:

$$\begin{aligned}
&u = \Delta\Omega r h'(\xi), \qquad v = \Delta\Omega r g(\xi) + \Omega_1 r, \qquad w = -2\,\Delta\Omega d h(\xi),\\
&\tau_{rr} = \eta\,\Delta\Omega\left(\widehat{RR}_0 + \frac{r^2}{d^2}\widehat{RR}_1\right), \qquad \tau_{r\theta} = \eta\,\Delta\Omega\frac{r^2}{d^2}\widehat{R\theta},\\
&\tau_{rz} = \eta\,\Delta\Omega\frac{r}{d}\widehat{RZ}, \qquad \tau_{\theta\theta} = \eta\,\Delta\Omega\left(\widehat{\theta\theta}_0 + \frac{r^2}{d^2}\widehat{\theta\theta}_1\right),\\
&\tau_{\theta z} = \eta\,\Delta\Omega\frac{r}{d}\widehat{\theta Z}, \qquad \tau_{zz} = \eta\,\Delta\Omega\widehat{ZZ},
\end{aligned} \tag{10}$$

The equations show that $\widehat{RR}_0 = \widehat{\theta\theta}_0$ if the initial conditions for the corresponding unsteady problem are the same. We have noted that the governing equations imply that v, $\tau_{r\theta}$, $\tau_{\theta z}$ are odd functions, u, w, $\tau_{\theta\theta}$, τ_{zz}, τ_{rr} are even functions of $\Delta\Omega$ in the sense that $(\Omega_1, \Omega_2) \to -(\Omega_1, \Omega_2)$. Note that in deriving the symmetry Re and W change sign.

The boundary conditions are:

$$
\begin{aligned}
&h = 0 \text{ at } \xi = 0 \text{ and } \xi = 1,\\
&h' = 0 \text{ at } \xi = 0 \text{ and } \xi = 1,\\
&g = 0 \text{ at } \xi = 0 \text{ and } g = 1 \text{ at } \xi = 1,\\
&\widehat{RR}_0 = 0 \text{ at } \xi = 0 \text{ and } \xi = 1,\\
&\widehat{ZZ} = 0 \text{ at } \xi = 0 \text{ and } \xi = 1.
\end{aligned}
\tag{11}
$$

Our system of equations is singular because we divide by $h(\xi)$ and $h(0) = 0$, we used a shooting method (RK4) to solve the equations and started the numerical integration using a power series solution at the origin which eliminates the apparent singularity.

$$
\begin{aligned}
&\widehat{RR}_0 = 2\alpha\xi + a_{12}\xi^2,\\
&\widehat{RR}_1 = 2W\alpha^2 + a_{21}\xi + a_{22}\xi^2,\\
&\widehat{R\theta} = 2W\alpha\beta + a_{31}\xi + a_{32}\xi^2,\\
&\widehat{RZ} = \alpha + a_{41}\xi + a_{42}\xi^2,\\
&\widehat{\theta\theta}_1 = 2W\beta^2 + a_{51}\xi + a_{52}\xi^2,\\
&\theta Z = \beta + a_{61}\xi + a_{62}\xi^2,\\
&\widehat{ZZ} = -4\alpha\xi + a_{72}\xi^2,\\
&h = \frac{\alpha}{2}\xi^2 + \frac{\gamma}{6}\xi^3 + a_{84}\xi^4,\\
&g = \beta\xi + a_{92}\xi^2 + a_{93}\xi^3,
\end{aligned}
\tag{12}
$$

where $\alpha = h''(0)$, $\beta = g'(0)$, $\gamma = h'''(0)$ and the a's are functions of α, β, γ only. After each shot we get $h(1)$, $h'(1)$ and $g(1) - 1$ and formulate a Jacobian matrix to iterate for α, β, γ using Newton's method so that we finally land on $h = 0$, $h' = 0$ and $g = 1$ at $\xi = 1$. This is the same procedure used by Larson [4] except that we are shooting for three variables.

Our computation agree with those given by Phan-Thien [1,2]. He presented the graphs of h, h', g but did not give graphs of the stresses. We have computed results for various values of Re and W and we present here

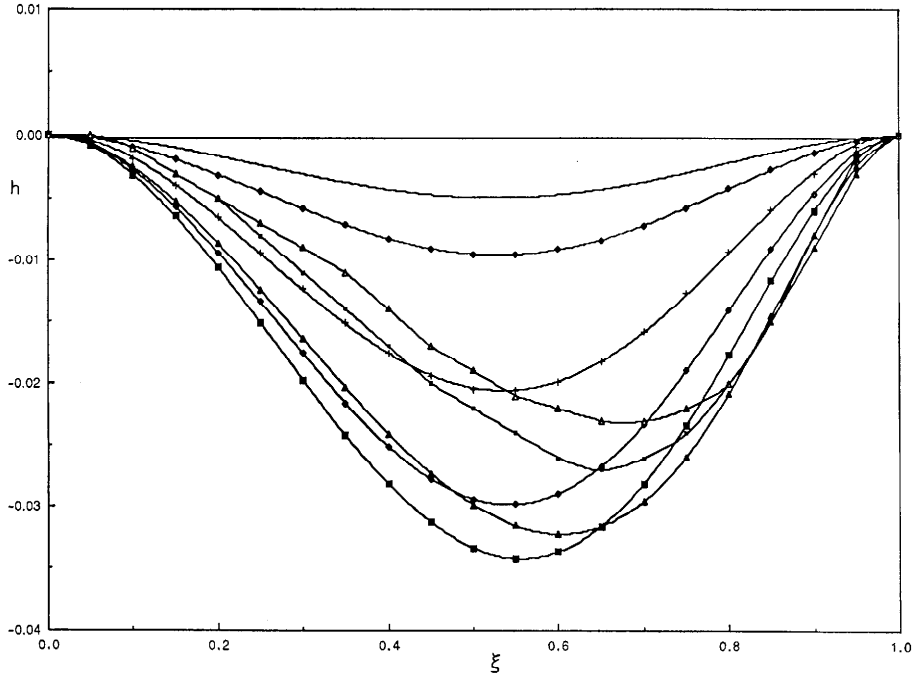

Fig. 1. $h(\xi)$ for Re: ● 1, ◆ 2, + 5, ◇ 10, ■ 20, ▲ 50, ▪ 100, △ 150 at $W = 1$.

graphs of the velocities, streamfunction, and all the stresses defined by (10) when $W = 1$ and $Re \leq 150$. We could not get convergent results for $W = 1$ and $Re > 180$ because of extreme sensitivity to initial guesses at high Reynolds number.

In Figs. 1 and 2 we have given the plots of $h(\xi)$ and $h'(\xi)$ giving the velocities u and w, $(10)_{1,3}$ of the secondary motion. The velocity v, $(10)_2$, is determined by $g(\xi)$ shown in Fig. 3. In Figs. 4 and 5 we show two of the stress-like quantities that seem important. The development of a boundary layer on the rotating wall at $\xi = 1$ as Re is increased at fixed W is strongly suggested by all these results. We shall see in the next section that these boundary layers appear in the elliptic regions rather than in the hyperbolic regions of flow. In thinking about stresses, given by (10) it is useful to think of r/d being a large multiplier as would be typical at the free edge $r = r_0$ of parallel plate rheometers. For example, in the parallel plate rheometer used by Broyer and Macosko [5] $25 < r/d < 250$. The shear stresses τ_{rz} and $\tau_{\theta z}$ are proportional to $\widehat{RZ}$ and $\widehat{\theta Z}$ with r/d as the constant of proportionality. The shear stress $\tau_{r\theta}$ is proportional to $\widehat{R\theta}$ in Fig. 4 with a constant of proportionality r^2/d^2. After comparing the three stresses we find surprisingly that there is a gigantic growth in the shear stress $\tau_{r\theta}$ in the boundary layer near

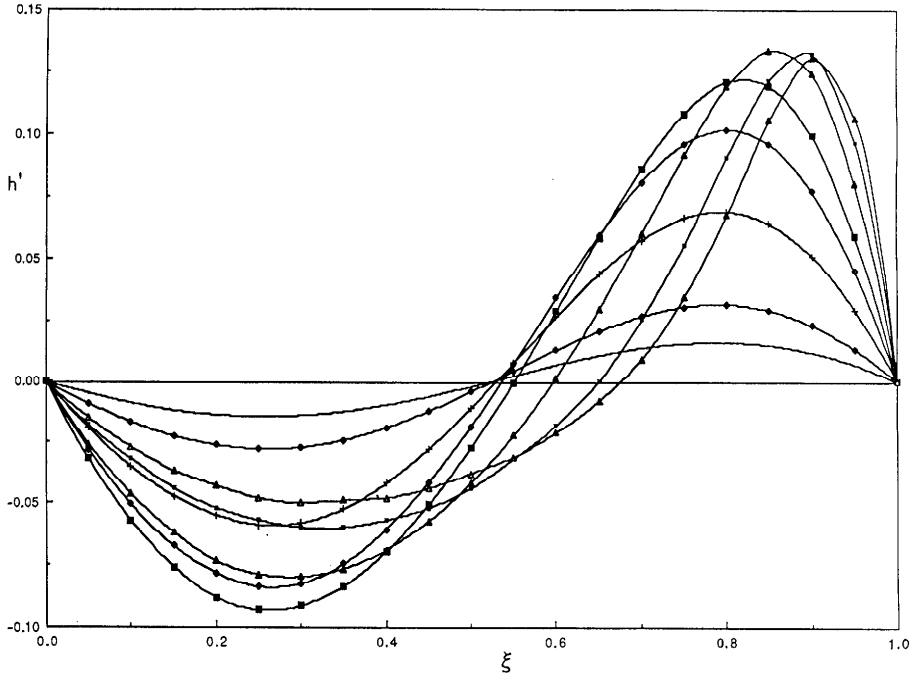

FIg. 2. $h'(\xi)$ for *Re*: ● 1, ◆ 2, + 5, ◇ 10, ■ 20, ▲ 50, ▪ 100, △ 150 at $W=1$.

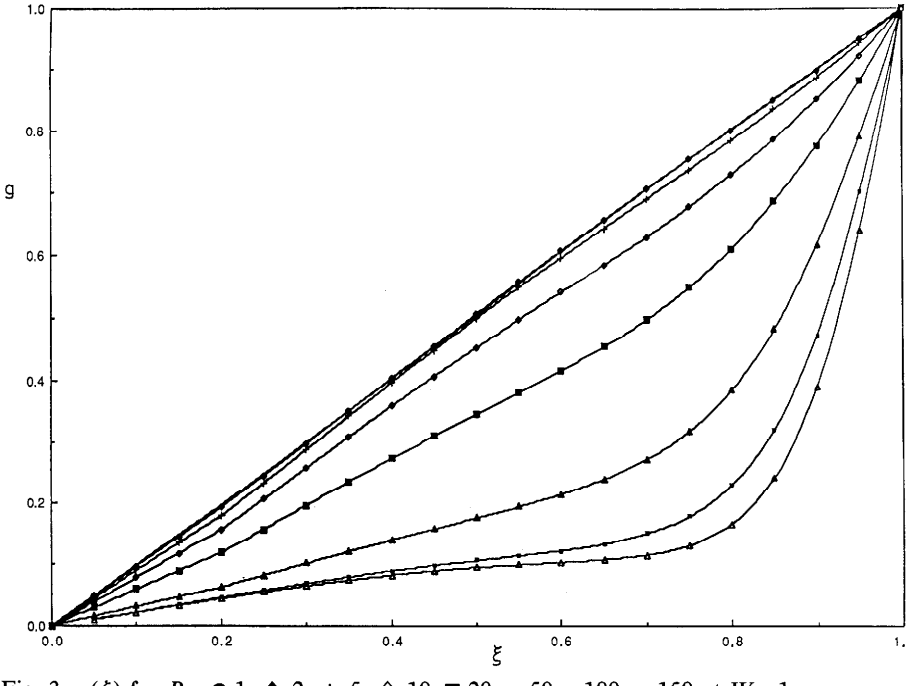

Fig. 3. $g(\xi)$ for *Re*: ● 1, ◆ 2, + 5, ◇ 10, ■ 20, ▲ 50, ▪ 100, △ 150 at $W=1$.

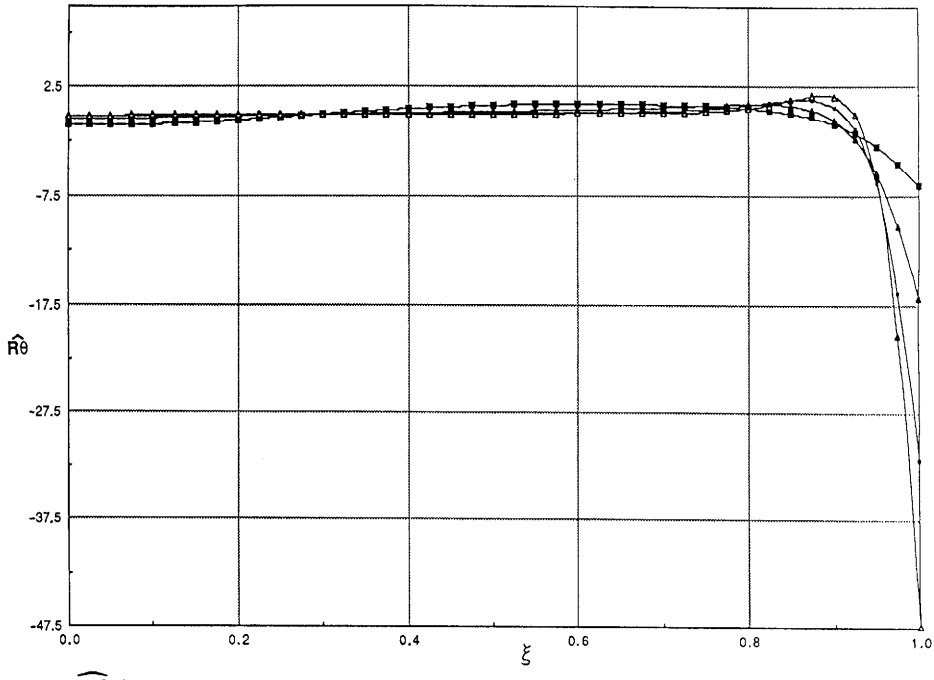

Fig. 4. $\widehat{R\theta}(\xi)$ for *Re*: ■ 20, ▲ 50, ▪ 100, △ 150 at $W=1$.

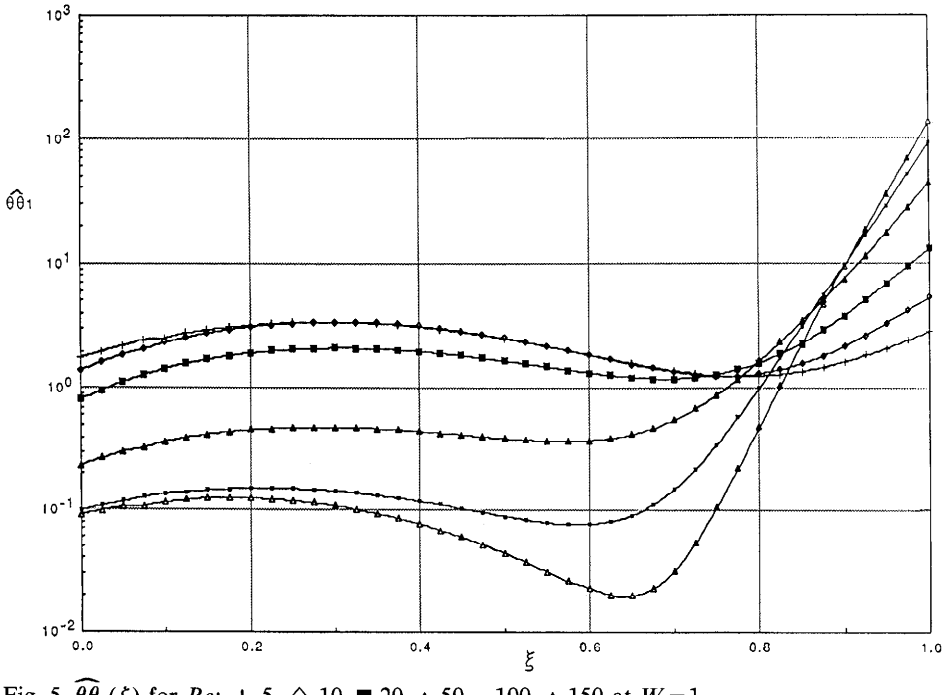

Fig. 5. $\widehat{\theta\theta_1}(\xi)$ for *Re*: + 5, ◇ 10, ■ 20, ▲ 50, ▪ 100, △ 150 at $W=1$.

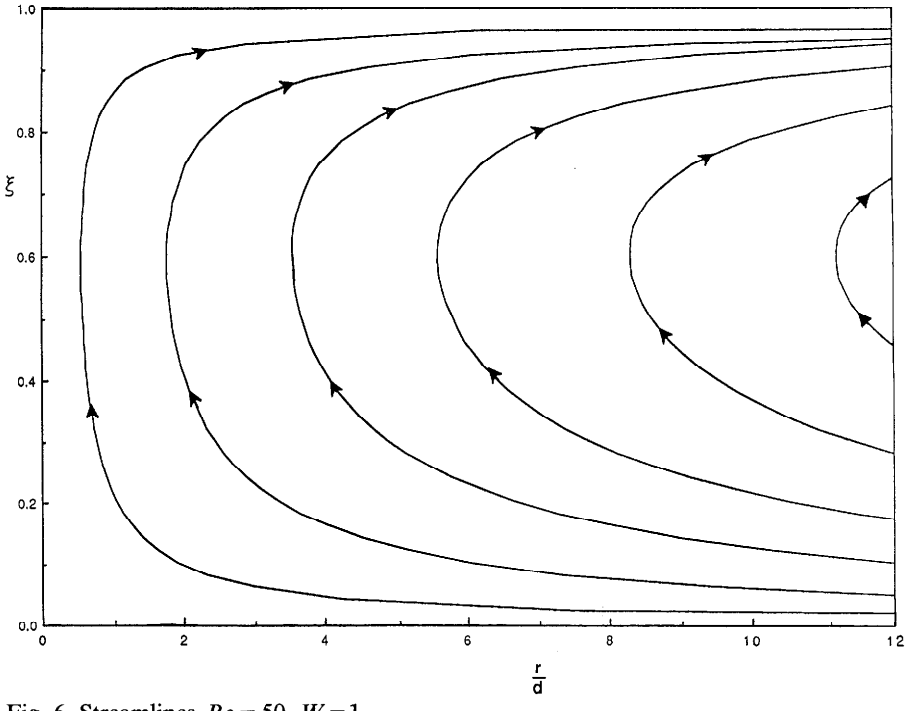

Fig. 6. Streamlines $Re = 50$, $W = 1$.

$\xi = 1$ when Re and r/d are large. The normal stresses τ_{rr} and $\tau_{\theta\theta}$ also scale with r^2/d^2 with amplitudes $\widetilde{RR}_1$ and $\widetilde{\theta\theta}_1$ (Fig. 5). The extra tension $\tau_{\theta\theta}$ near $\xi = 1$ at the edge of parallel plate rheometers can be truly enormous.

For small Reynolds number in the operating range $10^{-5} < Re < 10^{-2}$ which are typical in the experiments of Broyer and Macosko [5] on the neck-in instability, the stresses $\tau_{\theta z}$ and $\tau_{\theta\theta}$ are huge compared to other stresses. They can be 10^4 times larger. This could be important for the generation of instability to non-axisymmetric disturbances (see Section 6). All the stresses moderate in the interior and grow strongly as Re is increased.

In Figs. 6 and 7 we have plotted the streamlines and isovorticity curves for $Re = 50$ and $W = 1$, where

$$\zeta = \frac{\partial u}{\partial z} - \frac{\partial w}{\partial r} = \Delta\Omega \frac{r}{d} h''(\xi). \tag{13}$$

The isovorticity curves are not interesting because they do not suggest the underlying hyperbolic structure of the dynamics. To see this we should have to look at the propagation of disturbed vorticity in steady flows perturbing this one. We expect to see the perturbed vorticity propagating along the

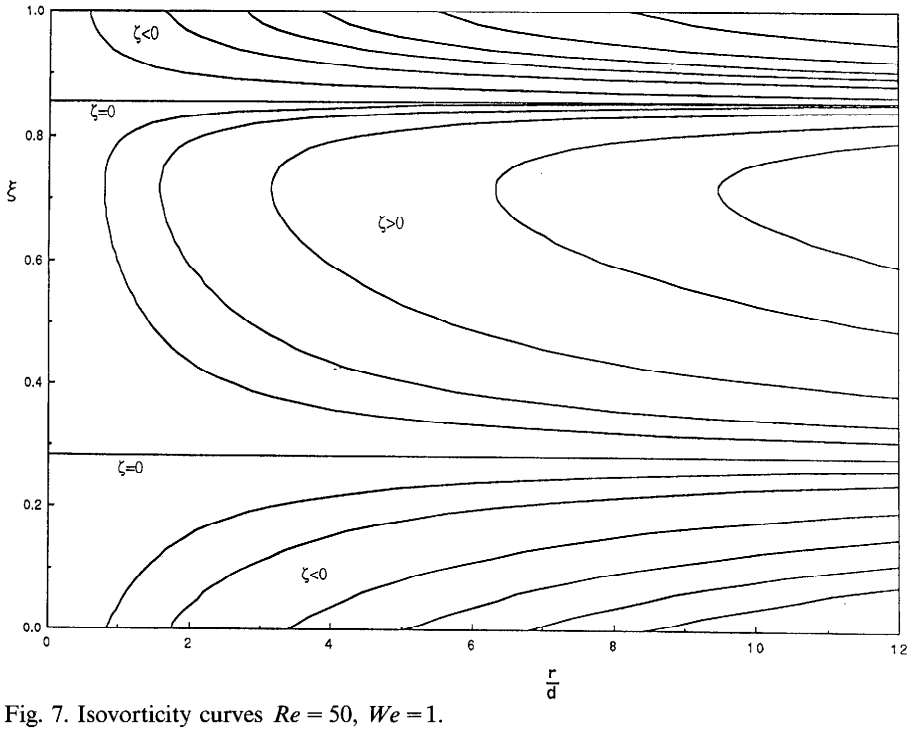

Fig. 7. Isovorticity curves $Re = 50$, $We = 1$.

characteristics in hyperbolic regions, as in the problems studied by Yoo and Joseph [6] and Ahrens et al. [7]. Some features of this type of perturbation are discussed in Section 6.

4. Change of type in the flow between rotating parallel plates

Now we look for the regions $B^2 - AC > 0$ defined in (7) where the vorticity is hyperbolic, we find

$$\Delta \overset{\text{def}}{=} \frac{B^2 - AC}{\Delta\Omega^2\eta^2} = \alpha(\xi)\frac{r^2}{d^2} + \beta(\xi), \tag{14}$$

where

$$\alpha(\xi) = (2\ Re\, hh' + \widehat{RZ})^2 - \left(4\ Re\, h^2 - \widehat{ZZ} - \frac{1}{W}\right)\left(Re\, h'^2 - \widehat{RR}_1\right)$$

$$\beta(\xi) = \left(4\ Re\, h^2 - \widehat{ZZ} - \frac{1}{W}\right)\left(\widehat{RR}_0 + \frac{1}{W}\right). \tag{15}$$

We found that $\beta(\xi) < 0$ in all cases. Using the boundary conditions (11) and the asymptotic expressions (12) we find that

$$\begin{aligned} \Delta &= -\alpha^2 \frac{r^2}{d^2} - \frac{1}{W^2}, \qquad z = 0, \\ \Delta &= -\delta^2 \frac{r^2}{d^2} - \frac{1}{W^2}, \qquad z = 1, \end{aligned} \tag{16}$$

where $\alpha = h''(0)$ and $\delta = h''(1)$. Moreover

$$\Delta = \beta(\xi) < 0 \text{ for } r = 0. \tag{17}$$

Therefore there is always an elliptic region close to the disks and close to the axis of rotation. Since $\beta(\xi) < 0$, the change of type occurs when $\alpha(\xi)$ changes sign. In our computations we found that $\alpha(\xi)$ changes sign four times when ξ goes from 0 to 1. Therefore there are two hyperbolic regions whose boundaries are defined by

$$r_c(\xi) = d\sqrt{-\frac{\beta(\xi)}{\alpha(\xi)}}, \tag{18}$$

where the limiting radius $r_c(\xi) \to \infty$ at the four roots of $\alpha(\xi)$ as shown in Fig. 8.

We used an asymptotic expansion in powers of Re, W (valid for moderately small Re and W) first used by Stewartson [8]. When the lower disk is fixed the leading terms of this expansion are

$$\begin{aligned} h &= -\frac{Re}{60}\xi^2(\xi-1)^2(\xi+2), \\ \widehat{RR}_0 &= 2h', \qquad \widehat{RR}_1 = 2Wh''^2, \\ \widehat{RZ} &= h'', \qquad \widehat{ZZ} = -4h'. \end{aligned} \tag{19}$$

Those five quantities are the only ones that are needed to see whether a change of type occurs at small Re and W. We obtain

$$\begin{aligned} \alpha(\xi) &= (2\ Re\ hh' + h'')^2 - \left(4\ Re\ h^2 + 4\ h' - \frac{1}{W}\right)(Re\ h'^2 - 2\ Wh''^2), \\ \beta(\xi) &= \left(4\ Re\ h^2 + 4\ h' - \frac{1}{W}\right)\left(2\ h' + \frac{1}{W}\right), \end{aligned} \tag{20}$$

where h is given in terms of ξ of $(19)_1$.

It is not hard to show, using (20) and after neglecting the smaller terms that

$\beta(\xi) < 0$,

$\alpha(\xi) < 0$ for $\xi_4 < \xi < 1$,

$\xi_2 < \xi < \xi_3$,

$0 < \xi < \xi_1$,

$\alpha(\xi) > 0$ for $\xi_1 < \xi < \xi_2$,

$\xi_3 < \xi < \xi_4$,

where the ξ_i $(i = 1, 2, 3, 4)$ are roots of $\alpha(\xi) = 0$ and such that $0 < \xi_1 < 0.237 < \xi_2 < 0.525 < \xi_3 < 0.808 < \xi_4 < 1$.

This agrees with our computations.

In Fig. 8 we plotted the hyperbolic regions and a net of characteristics for a Reynolds number of 50 and Weissenberg number of 1.

The effect of the parameters on the size and position of the regions of hyperbolicity are shown in Figs. 9 and 10. In general the hyperbolic regions move in and their width decreases as the Weissenberg number W is increased at a fixed value of Re. At a fixed Weissenberg number the regions move in if the Reynolds number is increased.

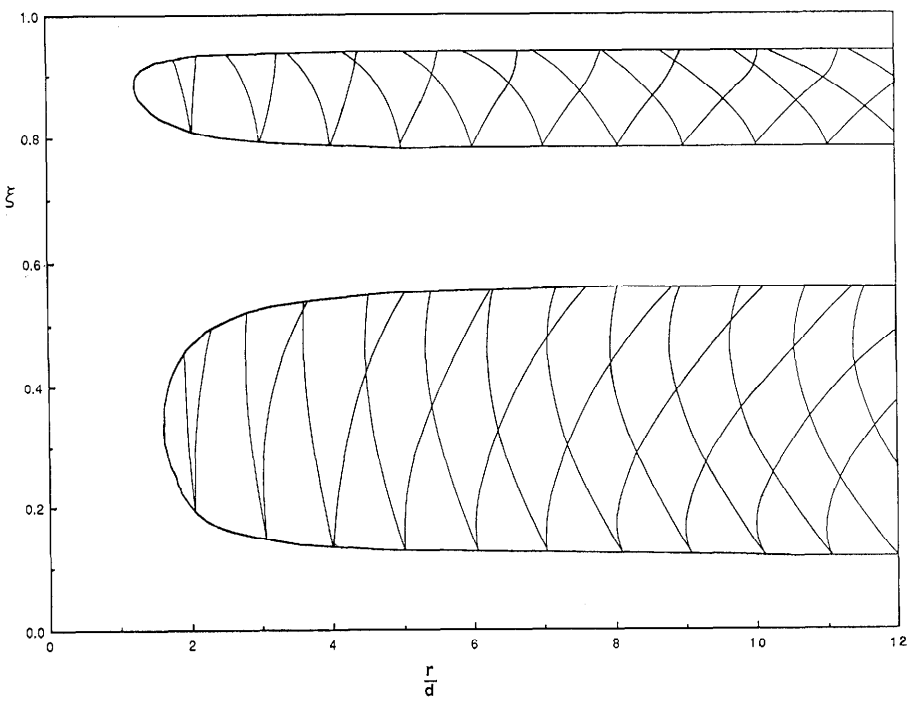

Fig. 8. Regions of hyperbolicity and characteristics, $Re = 50$ and $W = 1$.

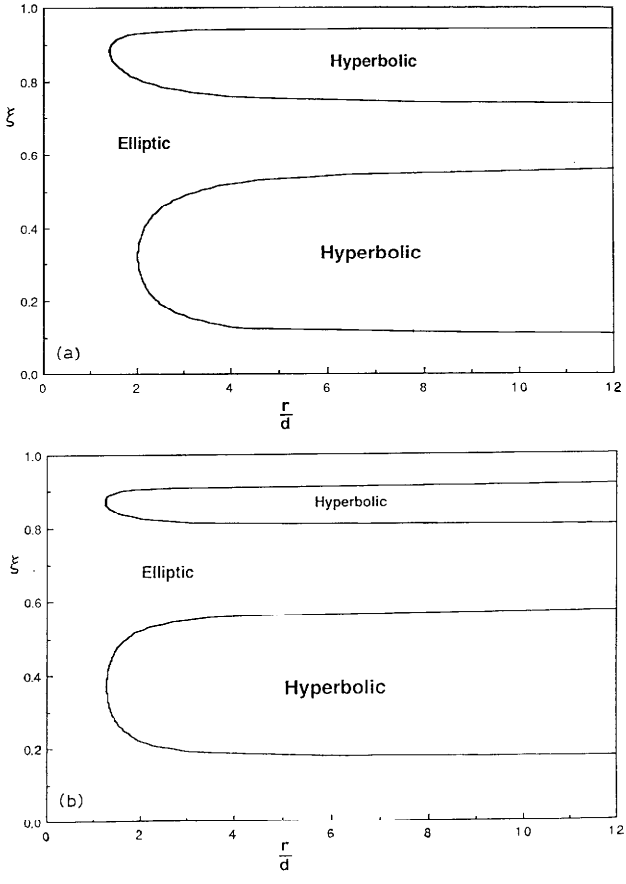

Fig. 9. (a) Hyperbolic regions $Re = 50$, $W = 0.6$; (b) $Re = 50$, $W = 1.8$.

The fact that we have two hyperbolic regions is physically hard to explain. It really comes from the mathematics: all the terms from $(15)_1$ have to be taken into account. At small Re and W for example $\alpha(\xi)$ changes sign if $G(\rho u^2 - \tau_{rr})$ changes sign, since the other terms can be neglected. In between the plates, u (like h') goes to 0 (see Fig. 2) and the stress τ_{rr} is dominant in the formula for $\alpha(\xi)$ therefore we get an elliptic region in the center also.

5. The viscoelastic Mach number

It may be more relevant here to introduce a local Mach number defined by

$$M = \frac{v}{c} = \frac{rG}{c} = \sqrt{W\,Re}\,\frac{r}{d}g(\xi). \tag{21}$$

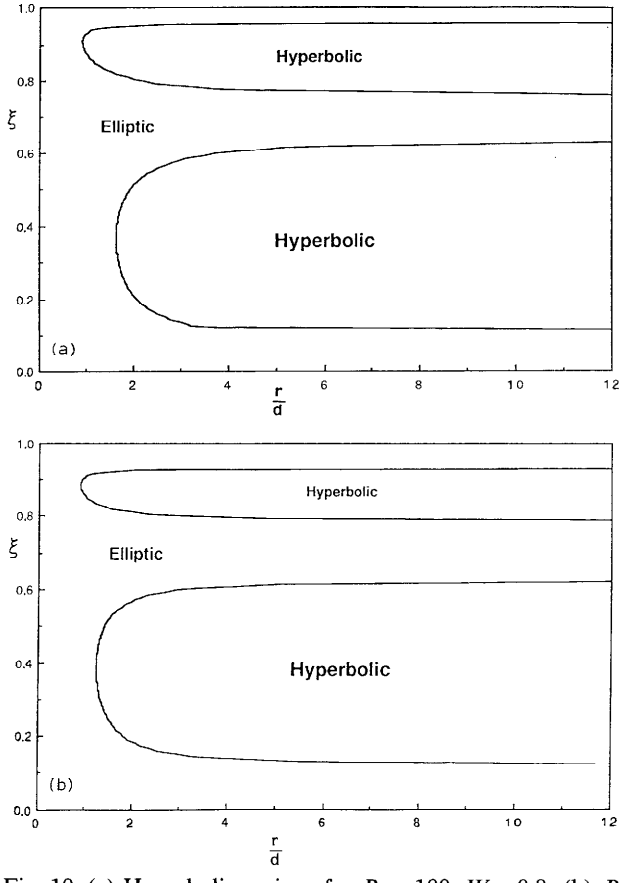

Fig. 10. (a) Hyperbolic regions for $Re = 100$, $W = 0.8$; (b) $Re = 100$, $W = 1.8$.

This Mach number increases with r and ξ. We want to check the value of the Mach number at the edge of each hyperbolic region, i.e. $M = M_c$ at the point where $r_c(\xi)$ is minimum. We now introduce

$$E = \frac{W}{Re} = \frac{\lambda \nu}{d^2}, \tag{22}$$

where E is the elasticity number.

We now think about one fluid, and we only vary the angular velocity Ω. Therefore E remains constant. Then we plot M_c as a function of Re (or similarly Ω). We did that in Fig. 11 for different elasticity numbers. We only plotted the smallest Mach number corresponding to the lower region. It appears that $M_c > 1$. Hence the Mach number is larger than one throughout the hyperbolic region.

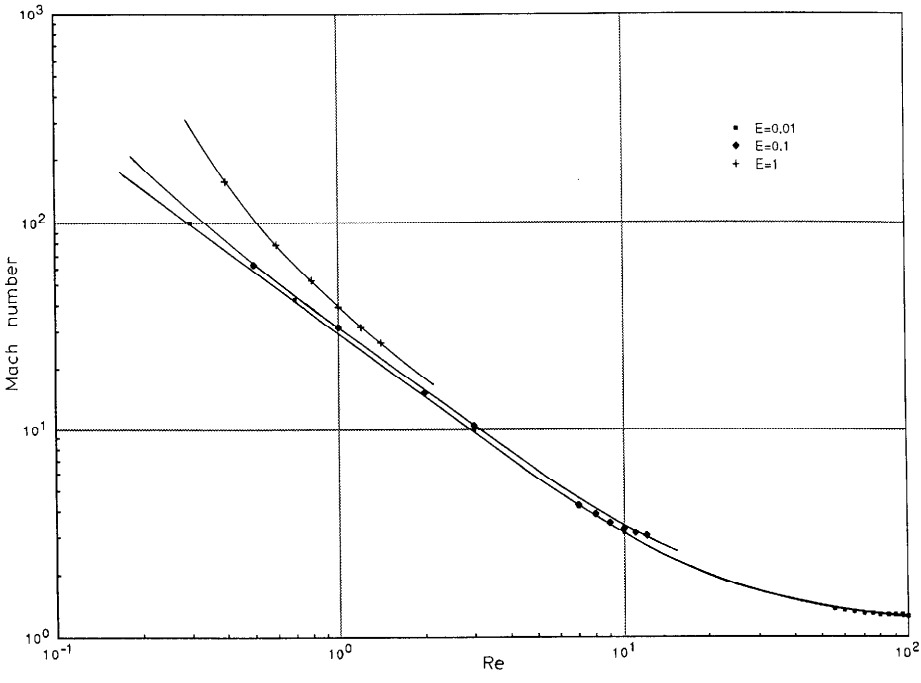

Fig. 11. Mach number at the edge vs. *Re* at different *E*.

6. Three dimensional perturbations of the similarity solution

Consider a small, but otherwise arbitrary perturbation of the similarity solution. For example, one could consider a perturbation induced by a wavy top plate $z = d + \epsilon \sin n\theta$ for small $\epsilon \to 0$. Each and every such perturbation gives rise to a linear system of equations; in particular the linearized vorticity equation for the upper convected Maxwell model is

$$A\frac{\partial^2\zeta}{\partial r^2} + \frac{B}{r^2}\frac{\partial^2\zeta}{\partial\theta^2} + C\frac{\partial^2\zeta}{\partial z^2} + \frac{2D}{r}\frac{\partial^2\zeta}{\partial r\,\partial\theta} + 2E\frac{\partial^2\zeta}{\partial r\,\partial z} + \frac{2F}{r}\frac{\partial^2\zeta}{\partial\theta\,\theta z} = \text{l.o.t.}, \tag{23}$$

where A, B, C, D, E, F depend on the basic flow:

$$\begin{aligned} A &= \rho u^2 - \tau_{rr} - G = A_0(z) + r^2 A_1(z), \\ B &= \rho v^2 - \tau_{\theta\theta} - G = B_0(z) + r^2 B_1(z), \\ C &= \rho w^2 - \tau_{zz} - G = C_0(z), \\ D &= \rho uv - \tau_{r\theta} = r^2 D_1(z), \\ E &= \rho uw - \tau_{rz} = rE_1(z), \\ F &= \rho vw - \tau_{\theta z} = rF_1(z), \end{aligned} \tag{24}$$

and

$$
\begin{aligned}
A_0(z) &= -\eta\,\Delta\Omega\widehat{RR}_0 - G,\\
A_1(z) &= \rho H_z^2 - \frac{\eta\,\Delta\Omega}{d^2}\widehat{RR}_1,\\
B_0(z) &= -\eta\,\Delta\Omega\widehat{\theta\theta}_0 - G,\\
B_1(z) &= \rho G^2 - \frac{\eta\,\Delta\Omega}{d^2}\widehat{\theta\theta}_1,\\
C_0(z) &= 4\,\rho H^2 - \eta\,\Delta\Omega\widehat{ZZ} - G,\\
D_1(z) &= \rho G H_z - \frac{\eta\,\Delta\Omega}{d^2}\widehat{R\theta},\\
E_1(z) &= -2\,\rho H H_z - \frac{\eta\,\Delta\Omega}{d}\widehat{RZ},\\
F_1(z) &= -2\,\rho H G - \frac{\eta\,\Delta\Omega}{d}\widehat{\theta Z}
\end{aligned}
\tag{25}
$$

are defined completely by the similarity solution.

Characteristic surfaces $\phi(r, \theta, z) = 0$ are those across which second derivatives can be discontinuous with continuity for lower order derivatives. After introducing characteristic coordinates into (23) we find that

$$
\begin{aligned}
&\big(A_0(z) + r^2 A_1(z)\big)\phi_r^2 + \left(\frac{B_0(z)}{r^2} + B_1(z)\right)\phi_\theta^2 + C_0(z)\phi_z^2\\
&\quad + 2\,rD_1(z)\phi_r\phi_\theta + 2\,rE_1(z)\phi_r\phi_z + 2\,F_1(z)\phi_\theta\phi_z = 0,
\end{aligned}
\tag{26}
$$

where

$$
\phi_r\,\mathrm{d}r + \phi_\theta\,\mathrm{d}\theta + \phi_z\,\mathrm{d}z = 0. \tag{27}
$$

In Section 4 we calculated the form of characteristic surfaces $\phi(r, z) = 0$ which are independent of θ. The coefficients of terms with ϕ_θ can be very large. We have not been successful in solving (26) and (27).

It is perhaps of interest to consider (26) in the case when $\Omega_1 = \Omega_2$, giving rise to rigid rotation. In this case (26) becomes

$$
\frac{\partial^2\zeta}{\partial r^2} + \frac{\partial^2\zeta}{\partial z^2} + \left(\frac{1}{r^2} - \frac{\Omega^2}{c^2}\right)\frac{\partial^2\zeta}{\partial\theta^2} = \text{l.o.t.}, \tag{28}
$$

giving rise to characteristic surfaces

$$
\phi_r^2 + \phi_z^2 + \left(\frac{1}{r^2} - \frac{\Omega^2}{c^2}\right)\phi_\theta^2 = 0. \tag{29}
$$

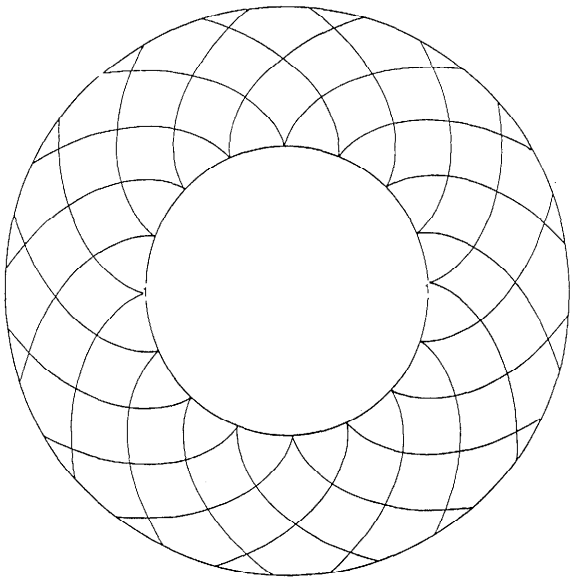

Fig. 12. Characteristics of rigid motion ($\Omega/C=1$, $\beta=1$) projection in the $r-\theta$ plane.

A three dimensional solution of (29) is

$$\phi(r, \theta, z) = \alpha z + \beta\theta + g(r), \tag{30}$$

where $g(r)$ satisfies

$$g'^2 + \alpha^2 + \beta^2\left(\frac{1}{r^2} - \frac{\Omega^2}{c^2}\right) = 0. \tag{31}$$

The condition $r > \Omega/c$ is sufficient to guarantee that the regions of flow with $r > r_c$ are hyperbolic. In Figs. 12 and 13 we plotted the characteristic surfaces (30) and (31).

It is perhaps of interest to recall that elastic cylinders under severe twists develop instabilities with spiral form, as in Fig. 12. The well known neck-in

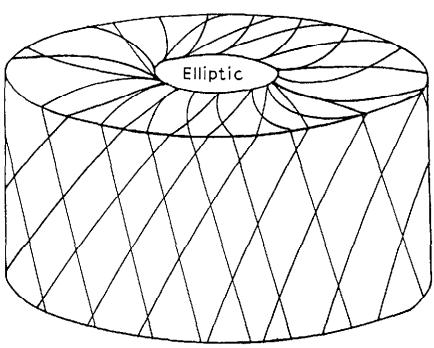

Fig. 13. Characteristic surfaces of rigid motion.

instability at the edge of a sample between rotating parallel plate disks develops spirals of this type before giving away. Broyer and Macosko [5] studied this instability and they showed that it was characterized by a critical velocity rather than a critical shear rate. This finding is unusual and it suggests a change of type. However the magnitude of the velocities in the experiments are several orders smaller than the ones needed to move the hyperbolic regions into the disk. We have not completely ruled out the possibility that this instability is connected to hyperbolicity in a way presently not understood by us, but on the face of it we cannot make the instability fit the change of type even given a wide latitude in the selection of the magnitude of the model parameters.

All this still leaves us in the dark about the physical consequences of the change of type we have found in the Phan-Thien solution.

7. Fluid driven by an accelerated surface

Menon found a similarity solution for the steady flow of a Maxwell fluid in an infinitely long cylinder of dimensionless radius $r = 1$ whose boundaries move with an axial velocity proportional to the axial coordinate $z (w(1) = z,\ u(1) = 0)$.

We assume axisymmetry again and note that

$$v = 0, \qquad \tau_{r\theta} = 0, \qquad \tau_{\theta z} = 0. \tag{32}$$

Equations (1) still apply and the similarity solution is given by

$$\begin{aligned} &u = f(r)/r, \qquad w = -zf'(r)/r, \\ &\tau_{rr} = -i(r), \qquad \tau_{\theta\theta} = -j(r), \\ &\tau_{rz} = -zk(r), \qquad \tau_{zz} = -g(r) - \tfrac{1}{2}h(r)z^2, \\ &p = p_0(r) + \tfrac{1}{2}p_1 z^2. \end{aligned} \tag{33}$$

where f, g, h, i, j, k, p_0 are functions of r only $(0 \le r \le 1)$ and p_1 is a constant pressure coefficient. The variables in (33) have been made dimensionless with a scale length based on the radius R of the cylinder and the velocity U of the accelerated surface. The problem depends on two dimensionless parameters, the Reynolds number $Re = UR/\nu$ and the Deborah number $De = \lambda U/R$ (where λ is the relaxation time of the fluid). The boundary conditions are

$$\begin{aligned} &f'(1) = 1, \qquad f(1) = 0, \\ &f(0) = 0, \qquad f'(0) = 0, \\ &i(0) = \frac{-f''(0)}{1 - De\, f''(0)}, \qquad g(0) = \frac{2\, f''(0)}{1 + 2\, De\, f''(0)}, \\ &k(0) = 0, \qquad h(0) = 0. \end{aligned} \tag{34}$$

To solve the equations, a rescaling technique is used, corresponding to the change of variables:

$$\xi = \sqrt{De\,|\,p_1\,|}\,\mathrm{r}, \qquad p^* = \frac{p_1}{|\,p_1\,|} = \mathrm{sign}(p_1),$$

$$f(r) = \frac{F(\xi)}{De^2\,|\,p_1\,|}, \qquad h(r) = |\,p_1\,|\,H(\xi),$$

$$k(r) = \sqrt{\frac{|\,p_1\,|}{De}}\,K(\xi), \qquad i(r) = \frac{I(\xi)}{De}, \tag{35}$$

$$g(r) = \frac{G(\xi)}{De}, \qquad Re = Re^*De^2\,|\,p_1\,|.$$

We are left with six non linear first order equations for F, F', G, H, I, K depending on the parameters Re^* and p^* together with the boundary conditions:

$$\begin{aligned} &F(0) = 0, \qquad F'(0) = 0, \\ &K(0) = 0, \qquad H(0) = 0, \\ &I(0) = \frac{-F''(0)}{1 - F''(0)}, \qquad G(0) = \frac{2\,F''(0)}{1 + 2\,F''(0)}, \end{aligned} \tag{36}$$

The solution is carried out using different values of $F''(0)$ and terminated when $F(\xi_0) = 0$ (ξ_0 corresponds to the rescaled position of the wall). The integration is initiated by an expansion in powers of ξ to remove the singularity at $\xi = 0$. Then determine De and p_1 from the stopping conditions:

$$\begin{aligned} 1 &= F'(\xi_0)\,De^{-3/2}\,|\,p_1\,|^{-1/2}, \\ 1 &= De^{-1/2}\,|\,p_1\,|^{-1/2}\xi_0. \end{aligned} \tag{37}$$

Our results are in good agreement with Larson's computations. Once the flow is determined we calculate $B^2 - AC$ using (5), $B^2 - AC$ has the same sign as Δ', where

$$\Delta' = \alpha(\xi)z^2 + \beta(\xi), \tag{38}$$

and $\alpha(\xi)$ and $\beta(\xi)$ are given by

$$\alpha(\xi) = \left(K - Re^*\frac{FF'}{\xi^2}\right)^2 - \left(\frac{F'^2Re^*}{\xi^2} + \tfrac{1}{2}H\right)\left(Re^*\frac{F^2}{\xi^2} + I - 1\right)$$

$$\beta(\xi) = \frac{1 - G}{De\,p_1}\left(Re^*\frac{F^2}{\xi^2} + I - 1\right). \tag{39}$$

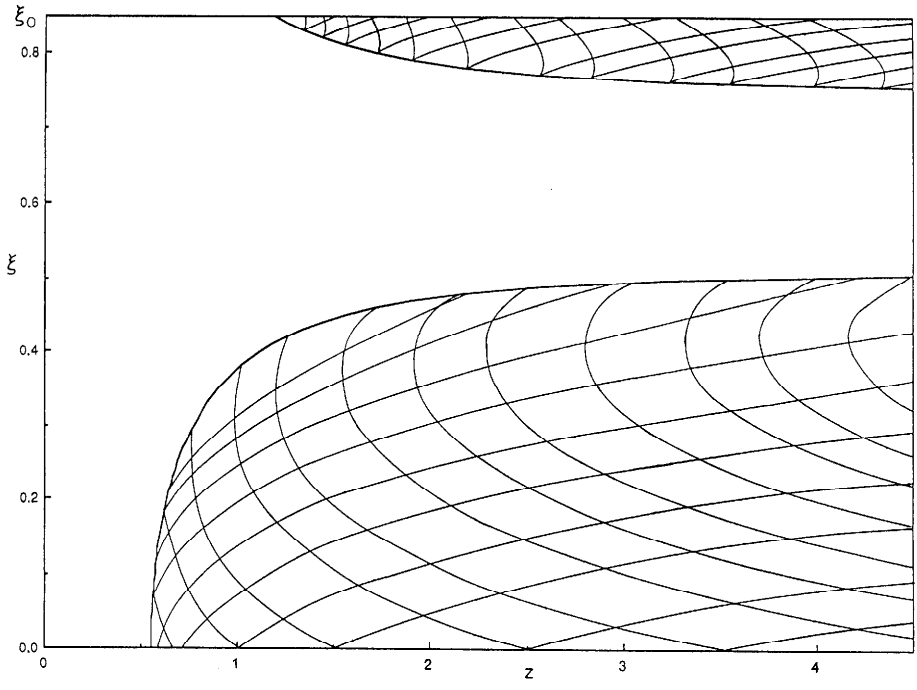

Fig. 14. Regions of hyperbolicity and characteristics, $De = 0.2$ and $Re = 9$.

Again we look at the signs of $\alpha(\xi)$ and $\beta(\xi)$ to determine where Δ' changes sign:

$$\beta(\xi) \leq 0 \qquad \text{for } 0 \leq \xi \leq \xi_0,$$
$$\alpha(\xi) \leq 0 \qquad \text{for } \xi_1 \leq \xi \leq \xi_2,$$
$$\alpha(\xi) \geq 0 \qquad \text{for } 0 \leq \xi \leq \xi_1 \text{ and } \xi_2 \leq \xi \leq \xi_0,$$

where ξ_1 and ξ_2 are roots of $\alpha(\xi) = 0$ $i = 1, 2$.

Therefore there are two regions that are hyperbolic, one close to the centerline, the other one close to the accelerated surface. These regions correspond to the domains of higher velocities. The regions appear when z is greater than a critical value $z_c(\xi)$ given by

$$z_c(\xi) = \sqrt{-\frac{\beta(\xi)}{\alpha(\xi)}} \,. \tag{40}$$

In Fig. 14 we plotted the regions of hyperbolicity and the characteristic grids on those regions.

As we increase the Reynolds number, the regions of hyperbolicity clearly move in toward the origin as shown in Figs. 15a–c.

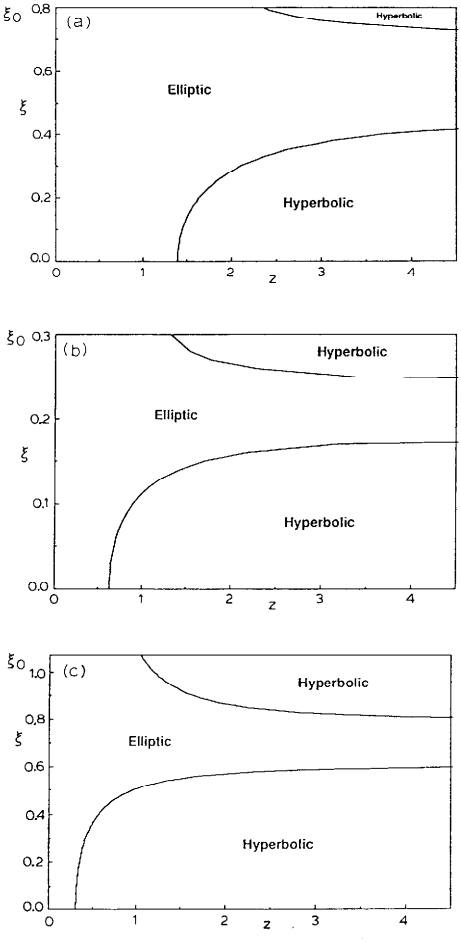

Fig. 15. (a) Hyperbolic regions $De = 0.1$, $Re = 3.84$; (b) $De = 0.1$, $Re = 9$; and (c) $De = 0.1$, $Re = 11.9$.

As the Deborah number is increased we observe the same behavior, but one region gets bigger (the one at the center line) and the other one gets smaller (the one close to the accelerated surface). This is shown in Figs. 16a to 16c.

8. Conclusions

We have shown that the similarity solution found by Phan-Thien for the flow of a viscoelastic fluid between parallel plates and by Menon of an accelerated tube flow produce a change of type in the vorticity equations. Those solutions can be used as exact standards to check computational algorithms designed to handle problems generated by changes of type.

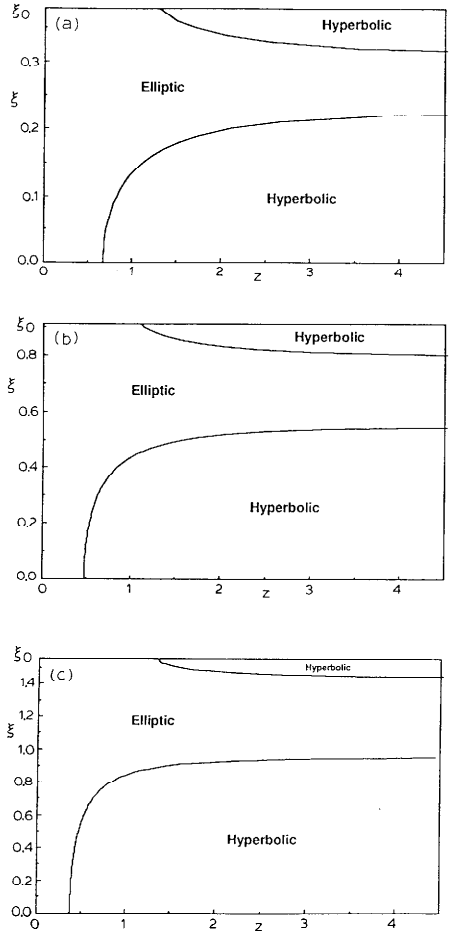

Fig. 16. (a) Hyperbolic regions $De = 0.115$, $Re = 10$; (b) $De = 0.24$; $Re = 10$; and (c) $De = 0.4$, $Re = 10$.

The problem of rotating parallel plates models the popular rheometrical device except that the effects of the free surface at the edge are neglected. Various transitions occur in such rheometers but none of them fit the requirements for a change of type of an upper convected Maxwell model. Some components of the stresses attain huge values at radii corresponding to the edge of real rheometers. The extra tension $\tau_{\theta\theta}$ is particularly large and may play a role in the well known neck-in instability which limits the use of rheometers to relatively small shear rates.

Acknowledgments

This work was sponsored by the Army Research Office, Mathematics and the National Science Foundation, Fluid Mechanics. Computer results were

obtained under a grant from the Academic Computing Services and Systems of the University of Minnesota.

References

1 N. Phan-Thien: Coaxial-disk flow and flow about a rotating disk of a Maxwellian Fluid, J. Fluid Mech., 128 (1983) 427–442.
2 N. Phan-Thien: Coaxial-disk flow of an Oldroyd-B fluid: exact solution and stability, J. Non Newtonian Fluid Mech., 13 (1983) 325–340.
3 R.K. Menon, M.E. Kim-E, R.C. Armstrong, R.A. Brown and J.F. Brady, Injection and suction of an upper-convected Maxwell fluid through a porous-walled tube, J. Non Newtonian Fluid Mech., 27 (1988) 265–297.
4 R.G. Larson: Viscoelastic inertial flow driven by an axisymmetric accelerated surface, J. Fluid Mech., 196 (1988) 449–465.
5 E. Broyer and C.W. Macosko: Comparison of cone-and-plate, bicone and parallel plates geometries for melt rheological measurements.
6 J.Y. Yoo and D.D. Joseph: Hyperbolicity and change of type in the flow of viscoelastic fluids through channels, J. Non Newtonian Fluid Mech., 19 (1985) 15–41.
7 M. Ahrens, J.Y. Yoo and D.D. Joseph: Hyperbolicity and change of type in the flow of viscoelastic fluids through pipes, J. Non Newtonian Fluid Mech., 24 (1987) 67–83.
8 K. Stewartson, Proc. Camb. Phil. Soc., Vol. 49, 1953, p. 333.